## Electronic Supplementary Information

# Thermoresponsive Chiral Plasmonic Nanoparticles

Yiyi Liu,[a] Tharaka Perera,[b] Qianqian Shi,[a] Zijun Yong,[a] Sudaraka Mallawaarachchi,[b] Bo Fan,[c] Julia Ann-Therese Walker,[a,d] Christopher J. Lupton[e,f] San H. Thang,[c] Malin Premaratne[b] and Wenlong Cheng*[a]

[a]Department of Chemical Engineering, Monash University, Clayton, Victoria 3800, Australia

[b]Advanved Computing and Simulation Laboratory (AχL), Department of Electrical and Computer Systems Engineering, Faculty of Engineering, Monash University, Clayton, Victoria 3800, Australia

[c]School of Chemistry, Monash University, Clayton, Victoria 3800, Australia

[d]Drug Delivery, Disposition and Dynamic, Monash Institute of Pharmaceutical Sciences, Parkville, Victoria 3052, Australia

[e]Biomedicine Discovery Institute, Monash University, Clayton, Victoria 3800, Australia

[f]ARC Centre of Excellence in Advanced Molecular Imaging, Monash University, Clayton, Victoria 3800, Australia

*Email: wenlong.cheng@monash.edu

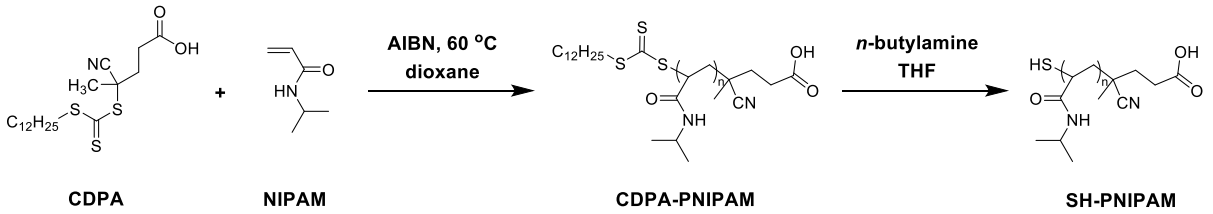


**Fig. S1.** Scheme of the synthesis of SH-PNIPAM.

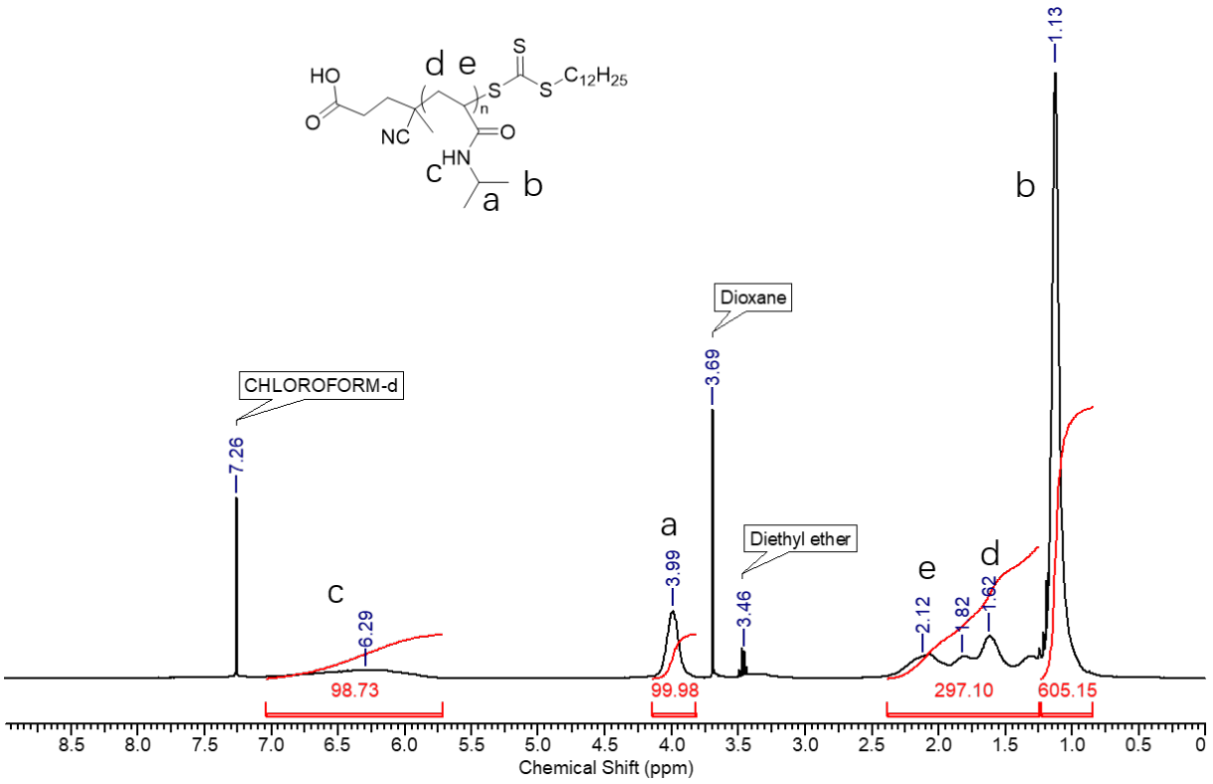


**Fig. S2.** $^{1}$H NMR spectrum CDPA-PNIPAM ($CDCl_3$, 400 MHz).

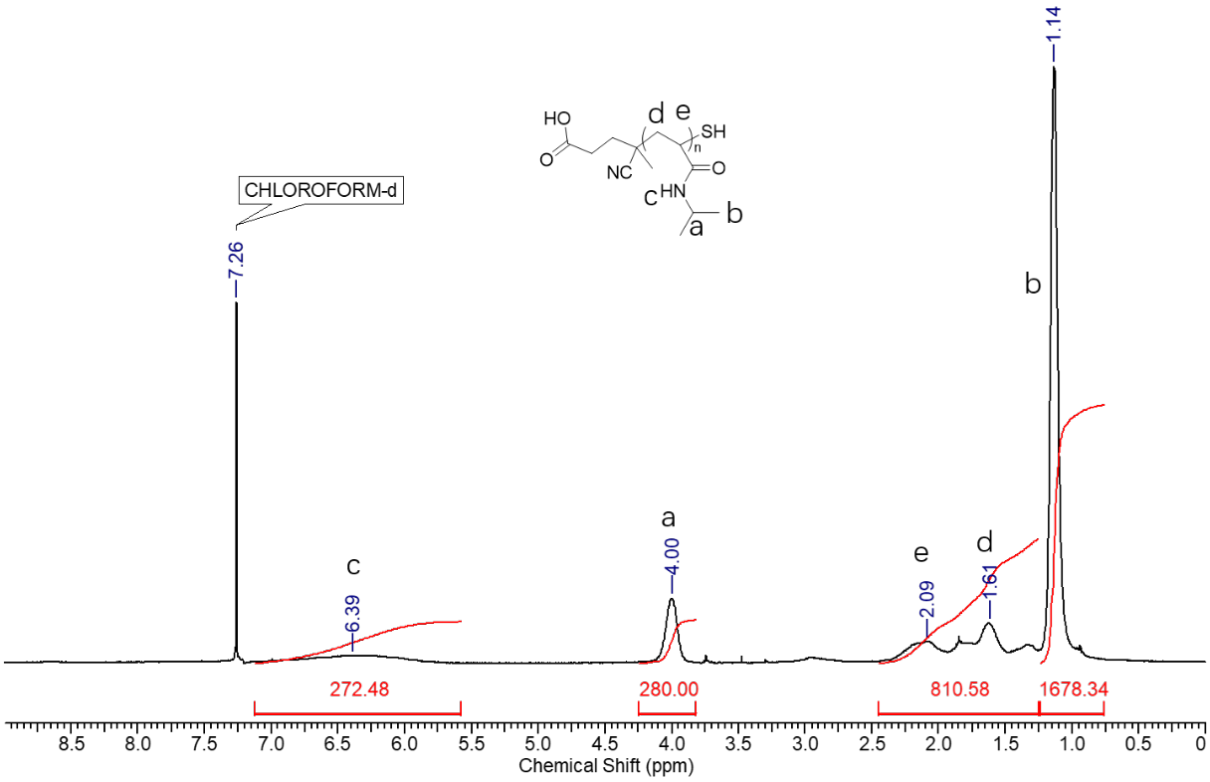


**Fig. S3.** $^{1}H$ NMR spectrum of SH-PNIPAM ($CDCl_3$, 400 MHz).

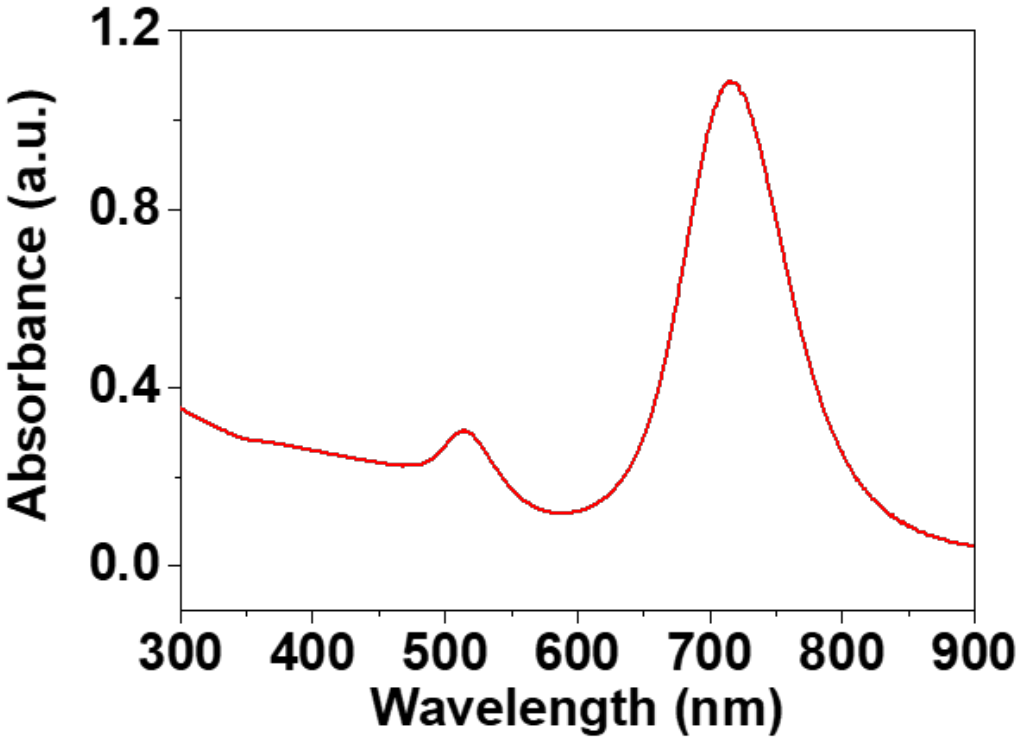


**Fig. S4.** UV-Vis spectrum of CTAB/NaOL protected AuNRs.

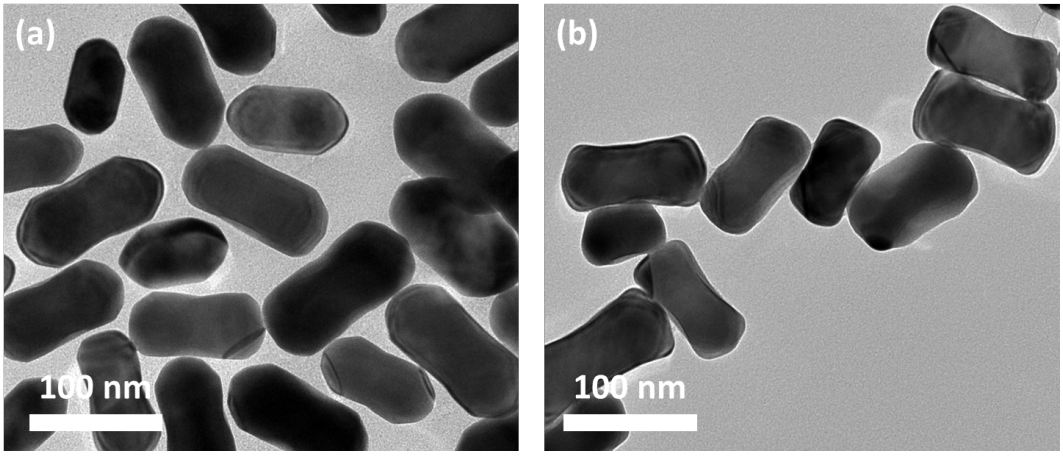


**Fig. S5.** TEM images of (a) D-AuNRs and (b) PNIPAM modified D-AuNRs.

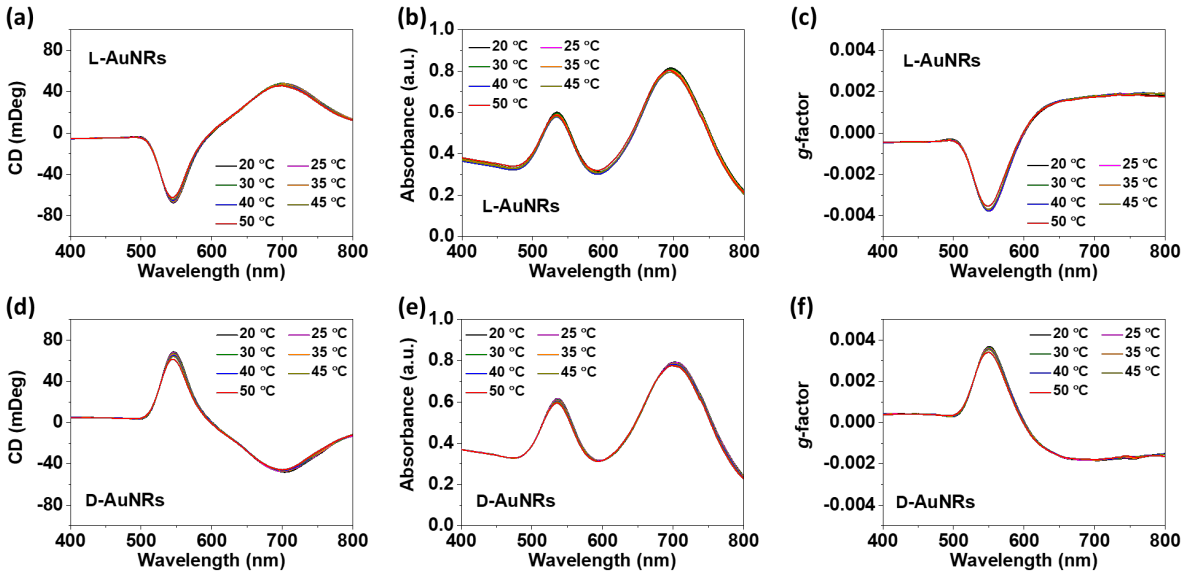


**Fig. S6.** Thermoresponsive behaviors of L-AuNRs and D-AuNRs without the modification of PNIPAM from 20 °C to 50 °C. CD spectra of (a) L-AuNRs and (d) D-AuNRs without the modification of PNIPAM from 20 °C to 50 °C, respectively. UV-Vis spectra of (b) L-AuNRs and (e) D-AuNRs without the modification of PNIPAM from 20 °C to 50 °C, respectively. *G*-factor plotting of (c) L-AuNRs and (f) D-AuNRs without the modification of PNIPAM from 20 °C to 50 °C, respectively.

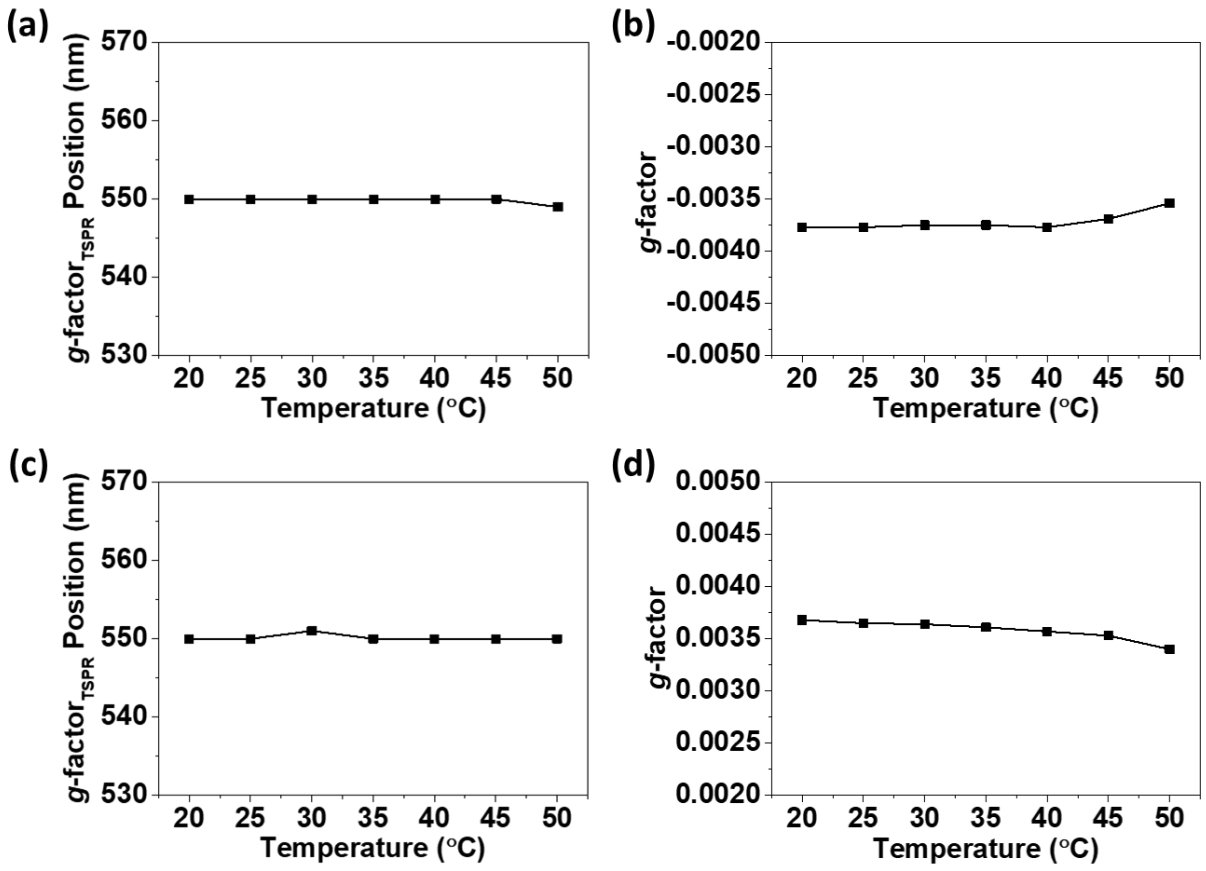


**Fig. S7.** Detailed analysis of *g*-factor$_{TSPR}$ bands changes for both L-AuNRs and D-AuNRs from 20 °C to 50 °C. *G*-factor$_{TSPR}$ bands positions of (a) L-AuNRs and (c) D-AuNRs *versus* the solution temperature. *G*-factor$_{TSPR}$ values of (b) L-AuNRs and (d) D-AuNRs *versus* the solution temperature.

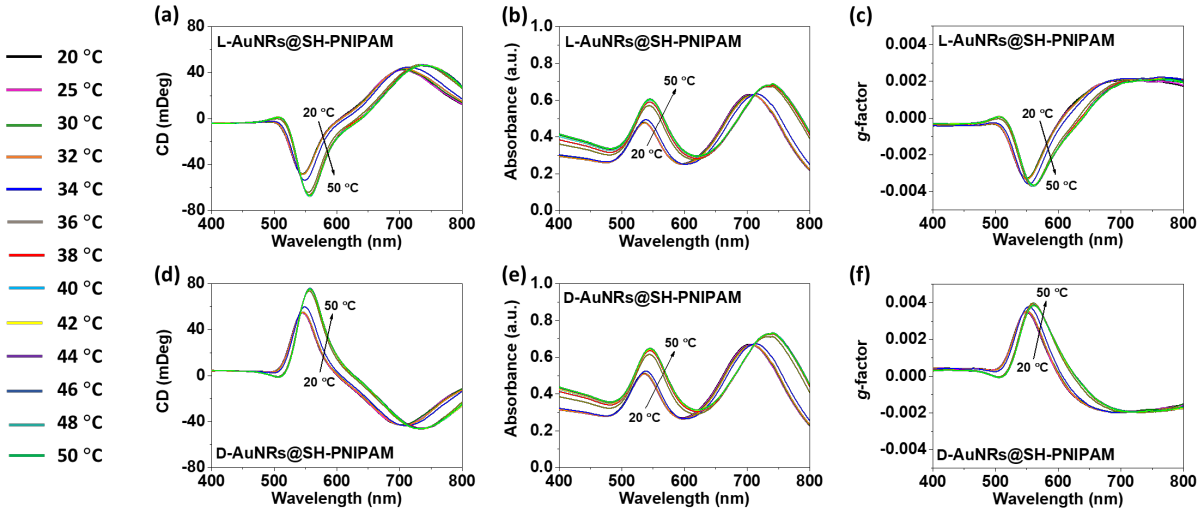


**Fig. S8.** Thermoresponsive behaviors of L-AuNRs and D-AuNRs with the modification of PNIPAM from 20 °C to 50 °C. CD spectra of (a) L-AuNRs and (d) D-AuNRs with the modification of PNIPAM from 20 °C to 50 °C, respectively. UV-Vis spectra of (b) L-AuNRs and (e) D-AuNRs with the modification of PNIPAM from 20 °C to 50 °C, respectively. *G*-factor plotting of (c) L-AuNRs and (f) D-AuNRs with the modification of PNIPAM from 20 °C to 50 °C, respectively.

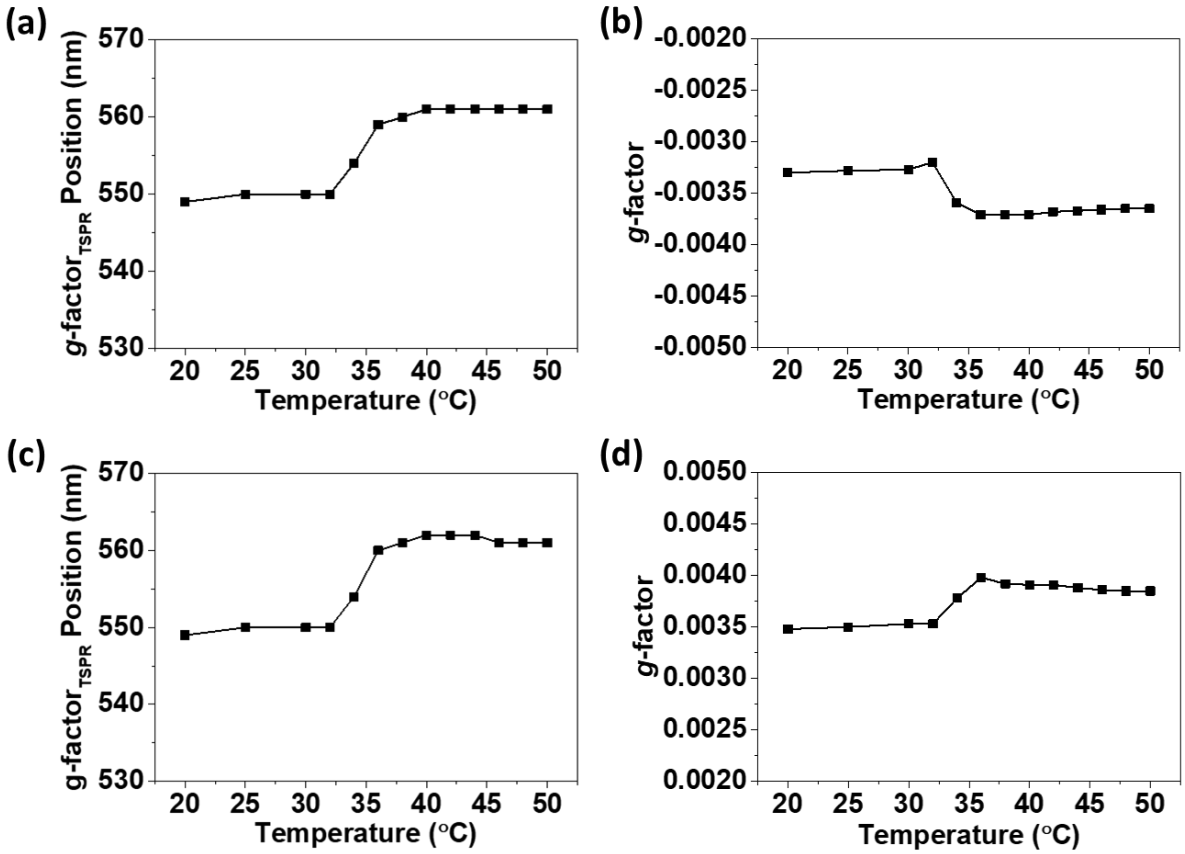


**Fig. S9.** Detailed analysis of *g*-factor$_{TSPR}$ bands changes for PNIPAM modified L-AuNRs and D-AuNRs from 20 °C to 50 °C. *G*-factor$_{TSPR}$ bands positions of PNIPAM modified (a) L-AuNRs and (c) D-AuNRs *versus* the solution temperature. *G*-factor$_{TSPR}$ values of PNIPAM modified (b) L-AuNRs and (d) D-AuNRs *versus* the solution temperature.

Multilevel mesh was used to numerically solve the Maxwell's equations. The maximum grid spacing of the mesh used for chiral nanorod was set to *2.25*nm (See Fig. S10a). For the background medium the grid spacing was set to $\lambda/8$, where $\lambda$ is the incident wavelength. A swept mesh with 5 elements was used for the perfect matched layer (See Fig. S10b).

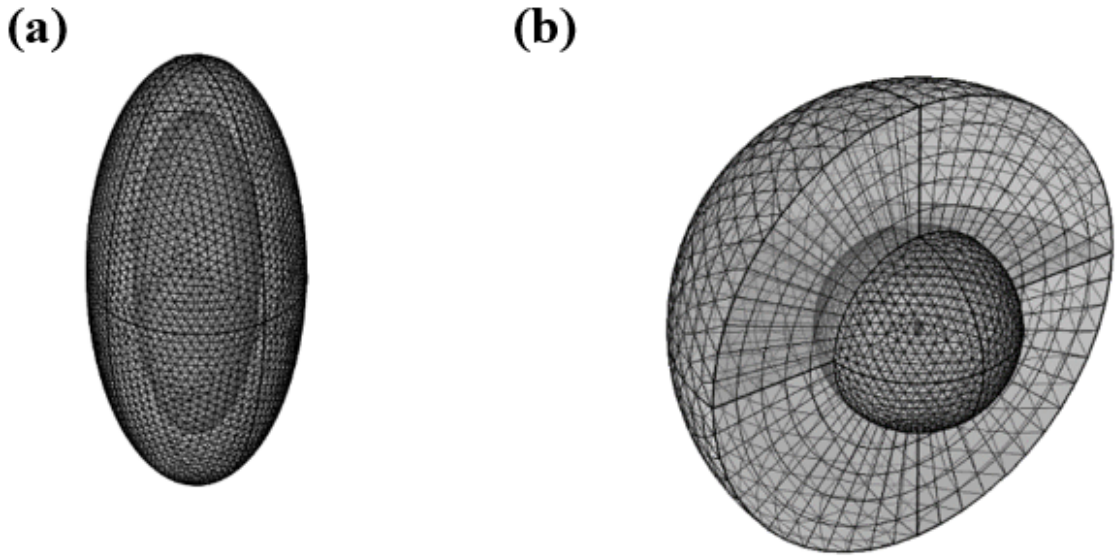


**Fig. S10.** Multilevel meshes used for numerical simulations. (a) Mesh used for chiral nanorod and (b) mesh used for the background medium and perfectly matched layer.

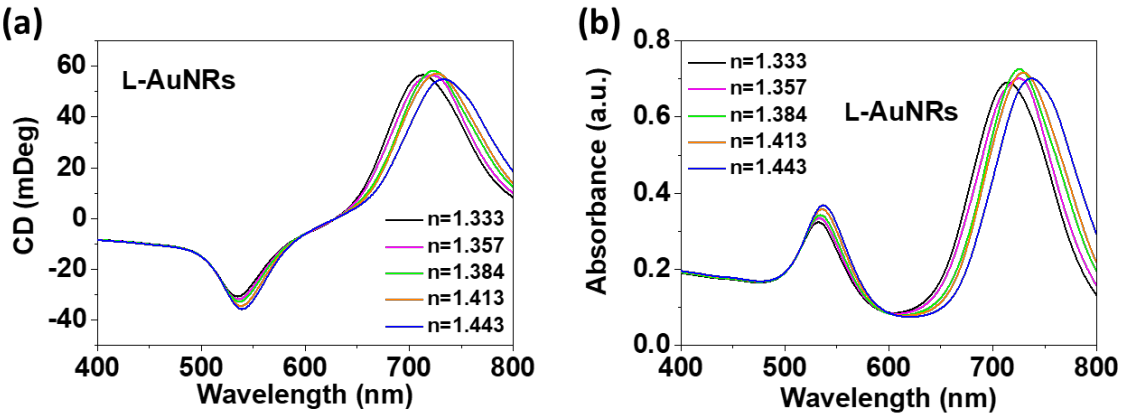


**Fig. S11.** Optical properties obtained by simulations of chiral AuNRs in five different dispersing mediums with increasing refractive indexes using the developed approximated model. (a) UV spectra and (b) CD spectra of L-AuNRs in 5 different dispersing mediums with increasing refractive indexes calculated using the developed approximated model, respectively.

| Water by Weight (wt%) | Glycerol by Weight (wt%) | Refractive Index |
|---|---|---|
| 100 | 0 | 1.333 |
| 80 | 20 | 1.357 |
| 60 | 40 | 1.384 |
| 40 | 60 | 1.413 |
| 20 | 80 | 1.443 |

**Fig. S12.** Corresponded refractive indexes of different water/glycerol mixture solutions.

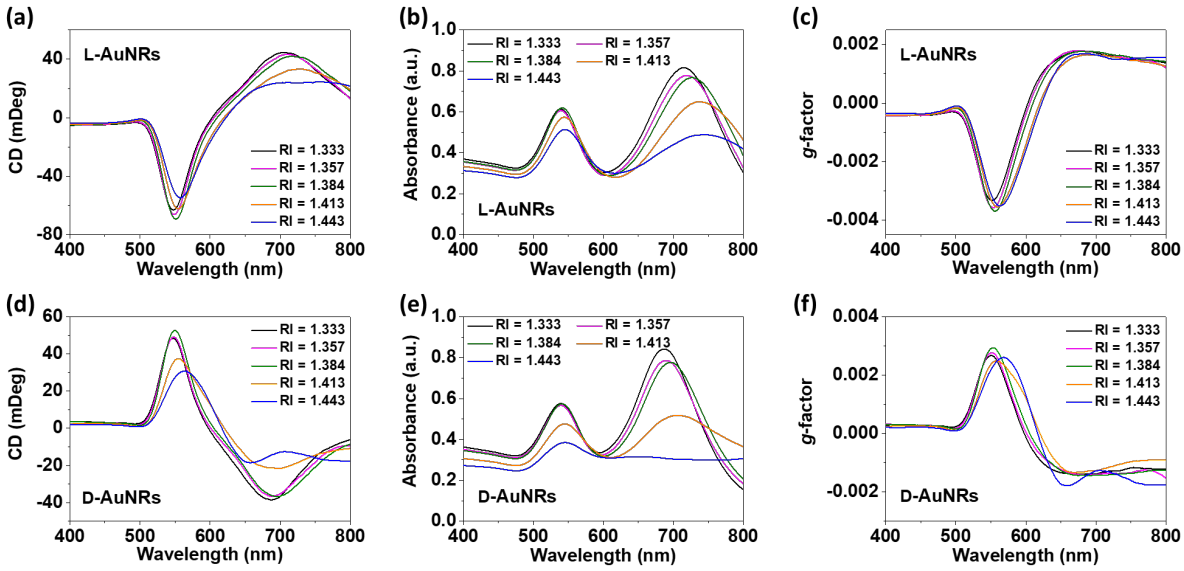


**Fig. S13.** Optical properties of chiral AuNRs in five different dispersing mediums with increasing refractive indexes. CD spectra of (a) L-AuNRs and (d) D-AuNRs in 5 different dispersing mediums with increasing refractive indexes, respectively. UV spectra of (b) L-AuNRs and (e) D-AuNRs in 5 different dispersing mediums with increasing refractive indexes, respectively. *G*-factor plotting of (c) L-AuNRs and (f) D-AuNRs in 5 different dispersing mediums with increasing refractive indexes, respectively.

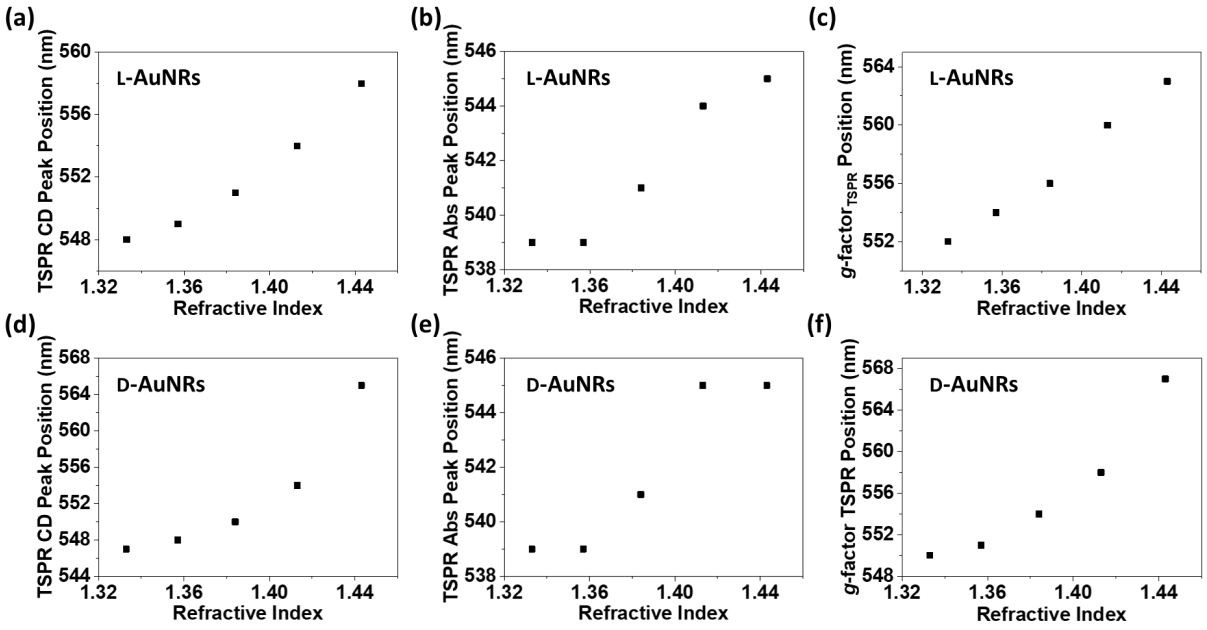


**Fig. S14.** Detailed analysis of optical properties of TSPR modes of chiral AuNRs in five different dispersing mediums with increasing refractive indexes. TSPR related PCD bands positions of (a) L-AuNRs and (d) D-AuNRs as a function of refractive index, respectively. TSPR mode UV absorption bands positions of (b) L-AuNRs and (e) D-AuNRs as a function of refractive index, respectively. TSPR mode corresponded *g*-factor bands positions of (c) L-AuNRs and (f) D-AuNRs as a function of refractive index, respectively.

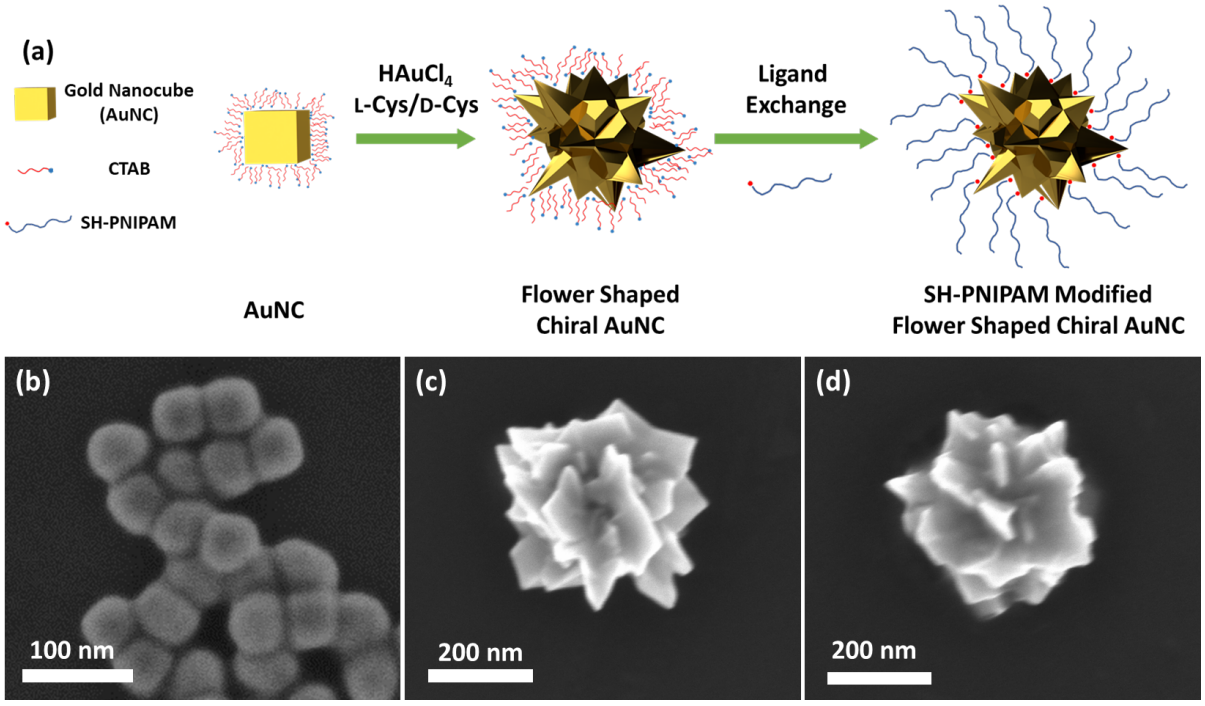


**Fig. S15.** Preparation of PNIPAM modified flower shaped chiral AuNCs. (a) Schematic illustration for the preparation of PNIPAM modified flower shaped chiral AuNCs. SEM images of (b) AuNCs, (c) flower shaped L-AuNC and (d) PNIPAM modified flower shaped L-AuNC.

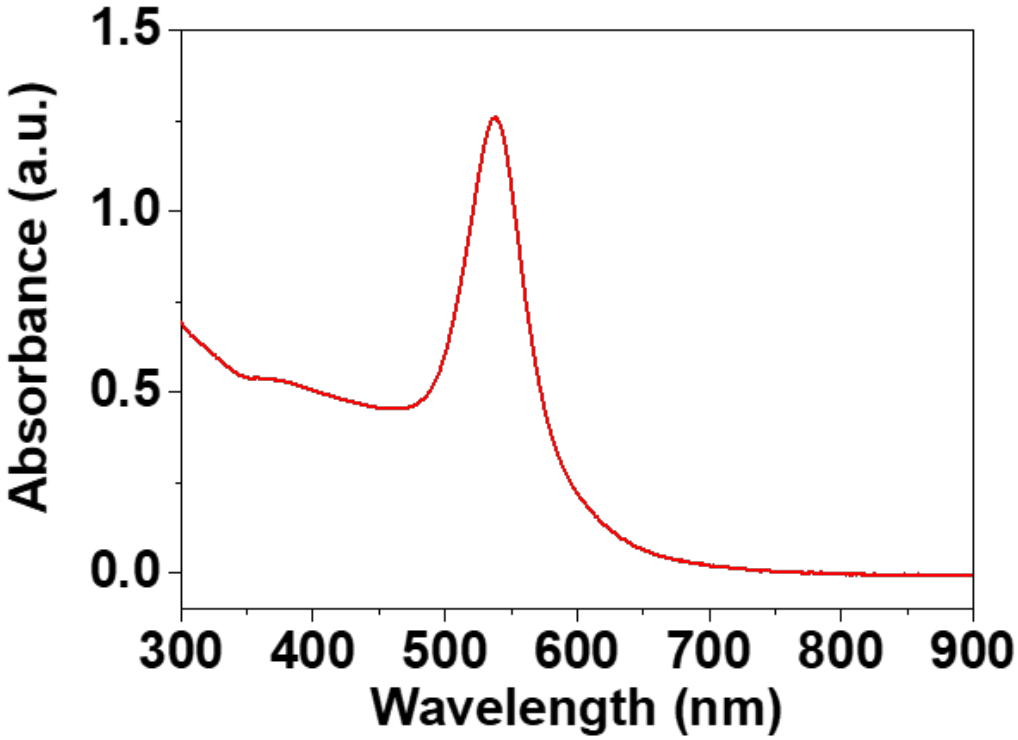


**Fig. S16.** UV-Vis spectrum of CTAB protected AuNCs.

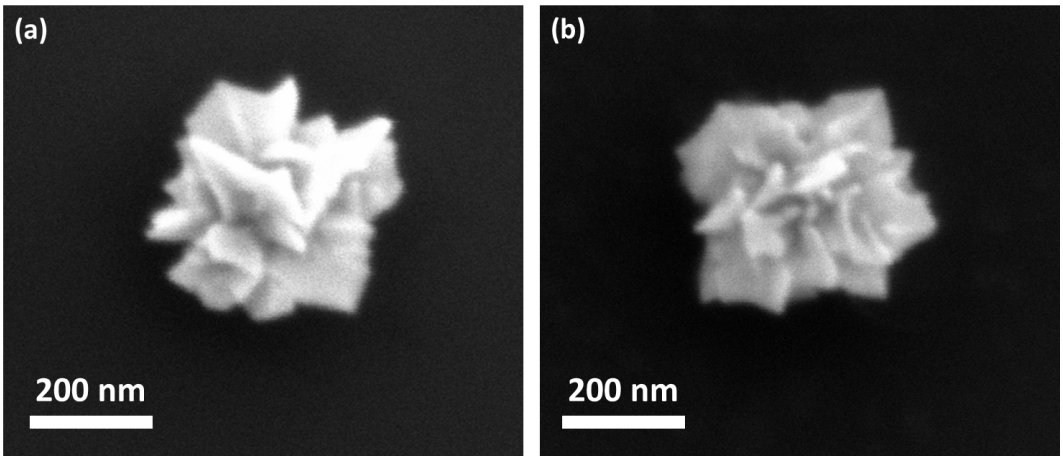


**Fig. S17.** SEM images of (a) flower shaped D-AuNC and (b) PNIPAM modified D-AuNC.

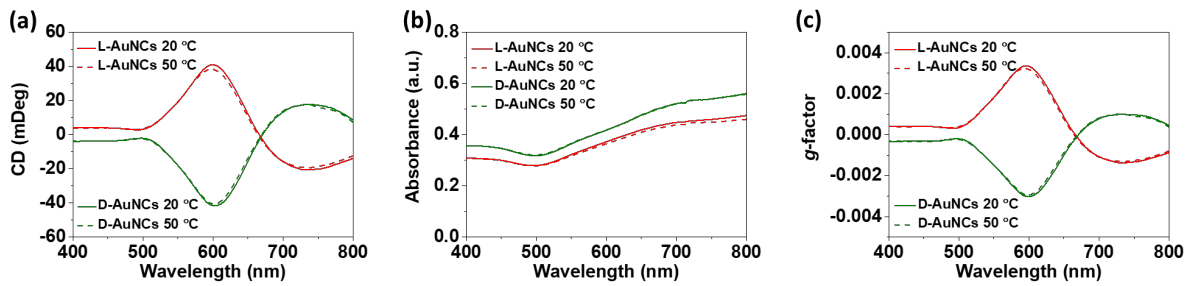


**Fig. S18.** Thermo-responsive behaviors of flower shaped chiral AuNCs without the modification of PNIPAM. (a) CD spectra of L-AuNCs and D-AuNCs without the modification of PNIPAM at 20 °C and 50 °C, respectively. (b) UV-Vis spectra of L-AuNCs and D-AuNCs without the modification of PNIPAM at 20 °C and 50 °C, respectively. (c) *G*-factor plotting of L-AuNCs and D-AuNCs without the modification of PNIPAM at 20 °C and 50 °C, respectively.

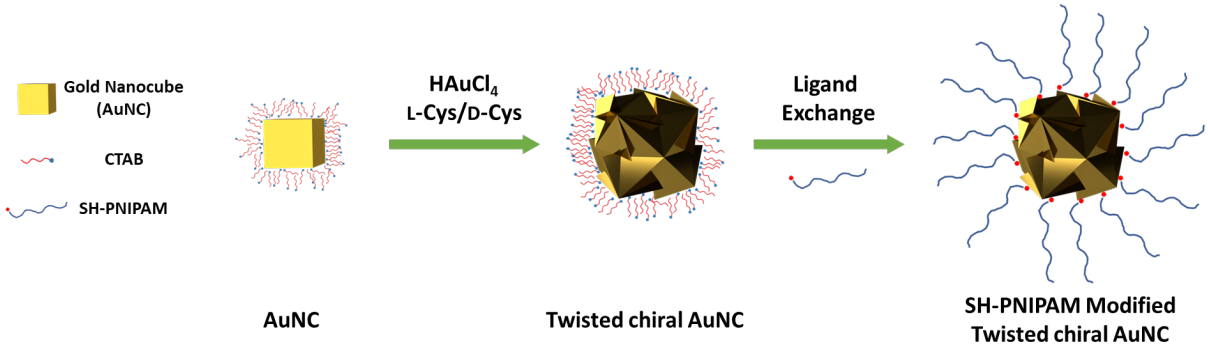


**Fig. S19.** Schematic illustration for the preparation of PNIPAM modified twisted chiral AuNCs.

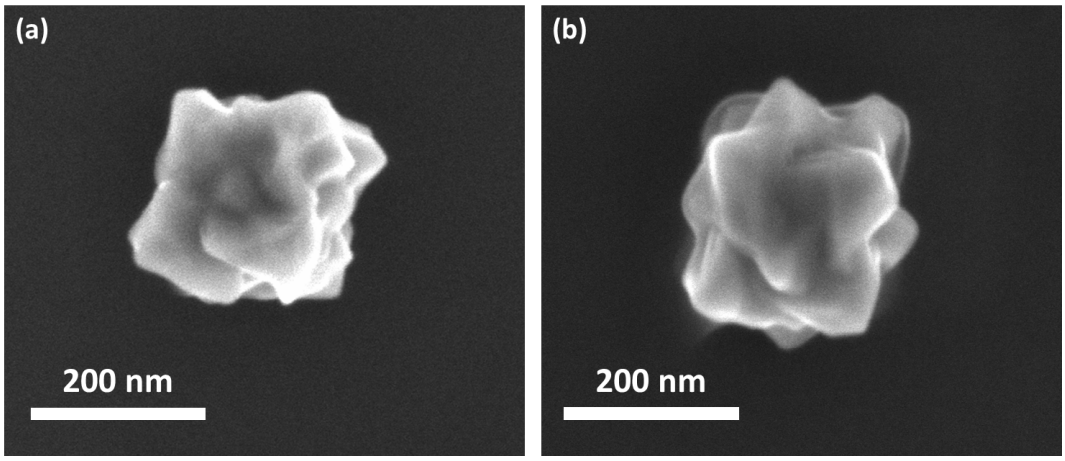


**Fig. S20.** SEM images of (a) twisted L-AuNC and (b) PNIPAM modified twisted L-AuNC.

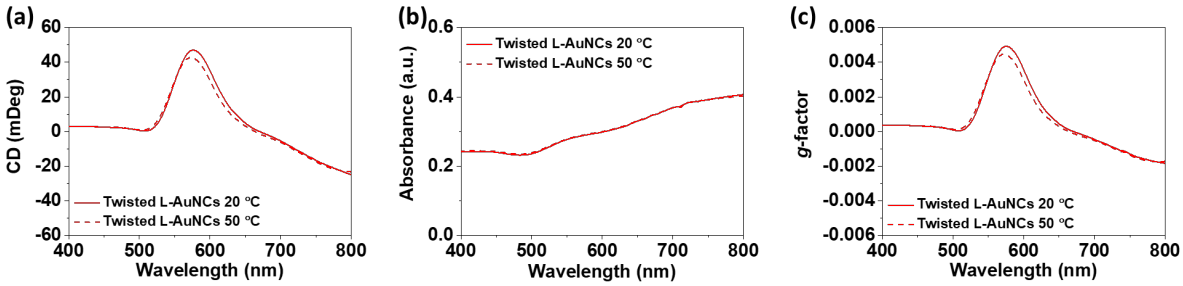


**Fig. S21.** Thermoresponsive behaviors of twisted chiral AuNCs without the modification of PNIPAM. (a) CD spectra of twisted L-AuNCs without the modification of PNIPAM at 20 °C and 50 °C, respectively. (b) UV spectra of twisted L-AuNCs without the modification of PNIPAM at 20 °C and 50 °C, respectively. (c) *G*-factor plotting of twisted L-AuNCs without the modification of PNIPAM at 20 °C and 50 °C, respectively.

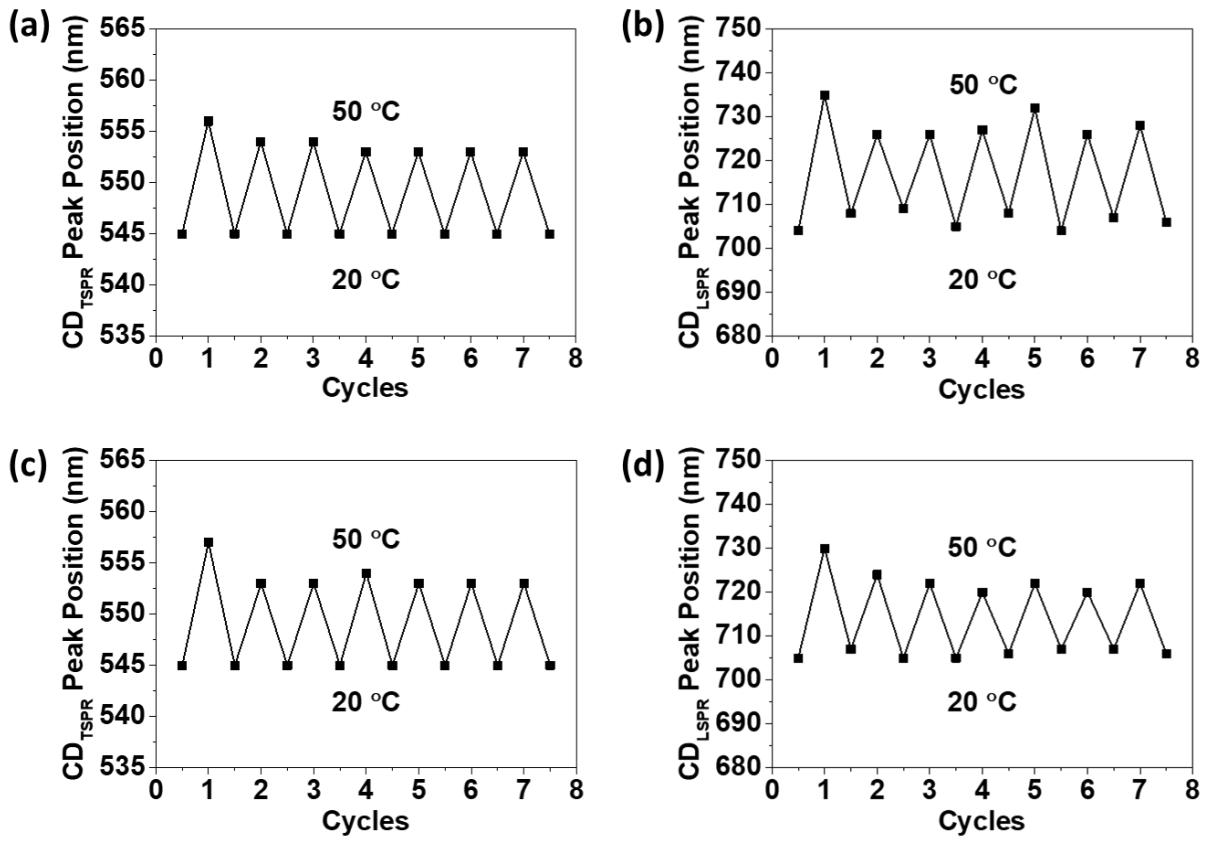


**Fig. S22.** Cycling tests for PNIPAM modified chiral AuNRs. Transverse mode CD peak positions of PNIPAM modified (a) L-AuNRs and (c) D-AuNRs as a function of the number of heating and cooling cycles. Longitudinal mode CD peak positions of PNIPAM modified (b) L-AuNRs and (d) D-AuNRs as a function of the number of heating and cooling cycles.

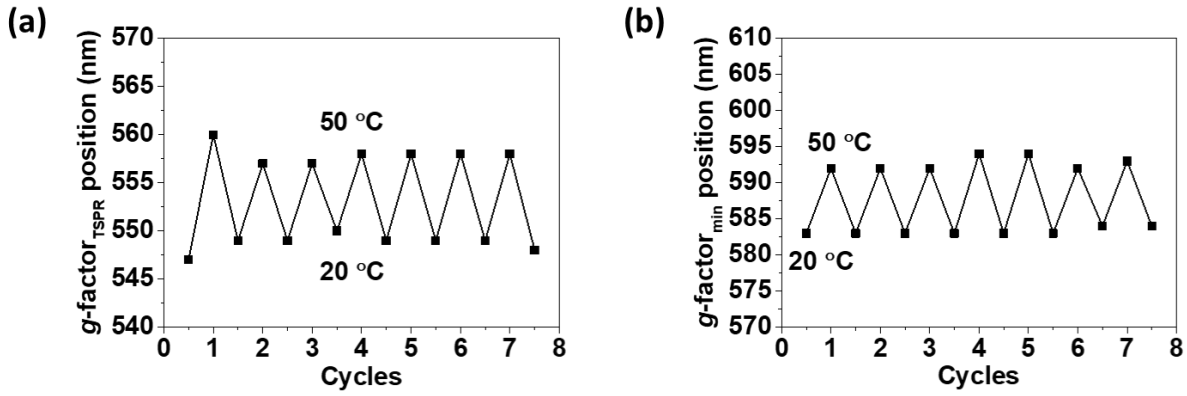


**Fig. S23.** Cycling tests for PNIPAM modified chiral AuNRs and flower shaped chiral AuNCs. (a) Transverse mode *g*-factor$_{min}$ peak positions of PNIPAM modified D-AuNRs as a function of the number of heating and cooling cycles. (b) *G*-factor$_{min}$ peak positions of PNIPAM modified flower shaped D-AuNCs as a function of the number of heating and cooling cycles.